The Influence of Anion on the Coarsening Kinetics of ZnO Nanoparticles

Zeshan Hu,[†] Gerko Oskam,[†,‡] R. Lee Penn,[§,||] Noshir Pesika,[⊥] and Peter C. Searson*[,†]

Department of Materials Science and Engineering, Department of Earth and Planetary Sciences, and Department of Chemical Engineering, Johns Hopkins University, Baltimore, Maryland 21218

Received: March 1, 2002; In Final Form: November 6, 2002

In solution phase synthesis of nanoparticles, processes such as coarsening and aggregation can compete with nucleation and growth in modifying the particle size distribution in the system. We report on the synthesis of ZnO nanoparticles from $Zn(CH_3CO_2)_2$, $ZnBr_2$, and $Zn(ClO_4)_2$ in 2-propanol. For synthesis from $Zn(CH_3CO_2)_2$ and $ZnBr_2$, nucleation and growth are fast and are followed by diffusion-limited coarsening. For synthesis from $Zn(ClO_4)_2$, diffusion-limited coarsening is observed at shorter times whereas at longer times the particle size increases more rapidly. The rate constant for coarsening at constant temperature increases in the order $Br^- < CH_3CO_2^- < ClO_4^-$ indicating that the rate is dependent on anion adsorption. The temperature dependence of the rate constant for coarsening is due to the temperature dependence of the solvent viscosity and the temperature dependence of the bulk solubility of ZnO.

Introduction

Solution phase methods have become widely used for the synthesis of crystalline semiconductor nanoparticles. In most cases these techniques involve nucleation and growth from homogeneous solution.[1−5] This approach has been used to synthesize nanoparticles of II−VI compounds (e.g., CdS,[6−8] CdSe,[6−8] PbS[9]), III−V compounds (InP,[10] InAs,[10] GaAs,[11]), and a wide range of metal oxides including TiO_2,[12] ZnO, [13−15] Fe_2O_3,[16] and PbO.[17]

To tailor the optical, electrical, chemical, and magnetic properties of nanoparticles for specific applications, it is essential to develop a fundamental understanding of the nucleation and growth process. Surprisingly, very little is known about the thermodynamics and kinetics of nucleation and growth of nanoparticles.

In solution phase synthesis, processes such as coarsening (also known as Ostwald ripening) and epitaxial attachment can compete with nucleation and growth in modifying the particle size distribution in the system. After injection of the precursors, nucleation is followed by particle growth until the supersaturation is depleted. If nucleation and growth are fast, coarsening and aggregation can dominate the time evolution of the particle size distribution. Aggregation is dependent on surface chemistry resulting in either oriented or random attachment of particles. Random aggregation usually leads to the formation of porous clusters of particles whereas epitaxial attachment of particles leads to the formation of secondary particles with complex shapes and unique morphologies.

Nucleation of metal oxide particles usually occurs by precipitation, involving the reaction of a soluble metal salt with hydroxide ions or water. The overall reaction for nucleation from a divalent metal salt MX_2 is of the following form:

$$MX_2 + 2YOH \rightarrow MO(s) + 2Y^+ + 2X^- + H_2O \quad (1)$$

where X represents the anion and Y corresponds to Na^+, K^+, NH_4^+, etc. In aqueous solution, growth usually proceeds rapidly with the formation of relatively large particles. In nonaqueous solvents the growth is generally much slower allowing controlled synthesis of nanoparticles.

Coarsening involves the growth of larger crystals at the expense of smaller crystals and is governed by capillary effects. Since the chemical potential of a particle increases with decreasing particle size, the equilibrium solute concentration for a small particle is much higher than for a large particle, as described by the Gibbs-Thompson equation. The resulting concentration gradients lead to transport of the solute (e.g., metal ions) from the small particles to the larger particles. The rate law for this process, derived by Lifshitz, Sloyozov, and Wagner (LSW),[18,19] is obtained by inserting the Gibbs-Thompson equation into Fick's first law:

$$\bar{r}^3 - \bar{r}_0^{\,3} = kt \quad (2)$$

where $\bar{r}$ is the average particle size, $\bar{r}_0$ is the average initial particle size, and t is time.

Attachment processes, such as epitaxial cluster aggregation, can lead to complex shapes and unique morphologies.[20−23] This mode of crystal growth is also known as topotactic attachment and is different from random aggregation since the particles attach epitaxially to form larger single crystals. This process is an example of a phase transformation in these systems; others include recrystallization and dissolution−reprecipitation.

In previous work we have shown that the coarsening of ZnO nanoparticles from $Zn(CH_3CO_2)_2$ in propanol follows the LSW rate law.[24] Here we report on the influence of the anion of the zinc salt on the coarsening kinetics.

Experimental Section

Particle Synthesis. The ZnO colloids were prepared from 2-propanol.[24,25] For a typical preparation, 1 mmol of a zinc salt

* Corresponding author. E-mail: searson@jhu.edu.
[†] Department of Materials Science and Engineering, JHU.
[‡] Present address: Departamento de Fisica Aplicada, CINVESTAV−IPN Unidad Merida, A. P. 73 Cordemex, Merida, Yucatan 97310, Mexico.
[§] Department of Earth and Planetary Sciences, JHU.
[||] Present address: Department of Chemistry, University of Minnesota, Minneapolis, MN 55455.
[⊥] Department of Chemical Engineering, JHU.

10.1021/jp020580h CCC: $25.00
Published on Web 03/18/2003

was dissolved in 80 mL of 2-propanol (Aldrich, spectrophotometric grade) in a covered flask under vigorous stirring at 50 °C. Three zinc salts were studied: zinc acetate dihydrate ($Zn(CH_3CO_2)_2 \cdot 2H_2O$, Aldrich, reagent grade), zinc bromide ($ZnBr_2$, Aldrich, reagent grade), and zinc perchlorate hexahydrate ($Zn(ClO_4)_2 \cdot 6H_2O$, Aldrich, reagent grade). After cooling to room temperature, 8 mL of the zinc salt solution was added to 64 mL of 2-propanol. A 0.02 M NaOH (Aldrich, reagent grade) solution was prepared by adding sodium hydroxide (Aldrich, reagent grade) to 2-propanol in a covered flask under vigorous stirring at 60 °C. After cooling to room temperature, 8 mL of the sodium hydroxide solution was added to 20 mL of 2-propanol. The covered flasks containing the zinc acetate solution and the sodium hydroxide solution were heated to the growth temperature in a water bath. The sodium hydroxide solution was then added to the zinc salt solution under vigorous stirring to give a total volume of 100 mL with 0.1 mmol zinc salt and 0.16 mmol NaOH. The overall nucleation reaction can be written as

$$ZnX_2 + 2NaOH \rightarrow ZnO + 2NaX + H_2O \qquad (3)$$

where $X = CH_3CO_2^-$, Br^-, or ClO_4^-. From the overall reaction it is seen that the synthesis is carried out with a 25% excess of Zn(II).

The combined influence of ClO_4^- and Br^- ions on particle growth was investigated by adding NaBr + NaOH to $Zn(ClO_4)_2$ solution, or by adding $NaClO_4$ + NaOH to $ZnBr_2$ solution. In the first case, 0.0206 g of NaBr was added to 8 mL of 12.5 mM $Zn(ClO_4)_2$ solution. To dissolve the NaBr, the solution was heated to 65 °C for about 4 h. The solution was then added to 64 mL of 2-propanol. Separately, 8 mL of 20 mM NaOH solution was added to 20 mL of 2-propanol. Finally the NaOH solution was added to the salt solution with both $Zn(ClO_4)_2$ and NaBr at 65 °C. In the second case, 25 mM $NaClO_4$ solution was prepared by dissolving 0.245 g of $NaClO_4$ in 80 mL of 2-propanol. Next, 8 mL of the $NaClO_4$ solution and 8 mL of 12.5 mM $Zn(ClO_4)_2$ solution were added to 56 mL of 2-propanol. The NaOH solution was then added to the salt solution at 65 °C.

Characterization. Absorption spectra were obtained using a Shimadzu UV-2101PC spectrophotometer. A slit width of 0.5 nm and a sampling interval of 0.2 nm s^{-1} were used to record the spectra from 275 to 400 nm. About 5 mL aliquots of the suspension were withdrawn during particle growth at predetermined time intervals and stored in an ice water bath prior to measurement. A blank solution of 2-propanol was used as reference.

Particle sizes were determined using a JEOL 3010 High-Resolution Transmission Electron Microscope (HRTEM). The microscope, operated at 300 keV, has a spatial point-to-point resolution of 0.17 nm. Samples were prepared by placing a drop of diluted suspension (10:1 by volume with 2-propanol) on a holey carbon-coated 2.3 mm copper grid and allowing the solvent to evaporate in air.

X-ray diffraction samples were prepared by compacting the powder in a zero-background quartz sample holder (The Gem Dugout Company, State College, PA). Measurements were performed on a Philips Model APD1700 diffractometer with a Cu Kα source and using a step size of 2 deg/s over the range $20 < 2\theta < 70$.

The solubility of ZnO was determined by atomic absorption spectroscopy (Perkin-Elmer Analyst 100). Samples were prepared as follows. ZnO powder (Aldrich, 99.9%) with particle sizes smaller than 1 μm was suspended in 2-propanol and ultrasonically agitated for 1 h. The suspension was then filtered over a 0.1 μm filter (Gelman Sciences) and the remaining solid was collected. The resulting ZnO particles with particle sizes larger than 0.1 μm were suspended in 2-propanol for 3 days at room temperature. The suspension was filtered over a 0.1 μm filter before analysis of the Zn(II) concentration with atomic absorption spectroscopy (AAS). The multiple filtration steps are necessary to remove nanometer-sized ZnO particles in the solution. Nanoparticles are also be detected by AAS, resulting in an overestimation of the ZnO solubility. Calibration was performed by preparing solutions of $Zn(ClO_4)_2$ in 2-propanol of known concentration.

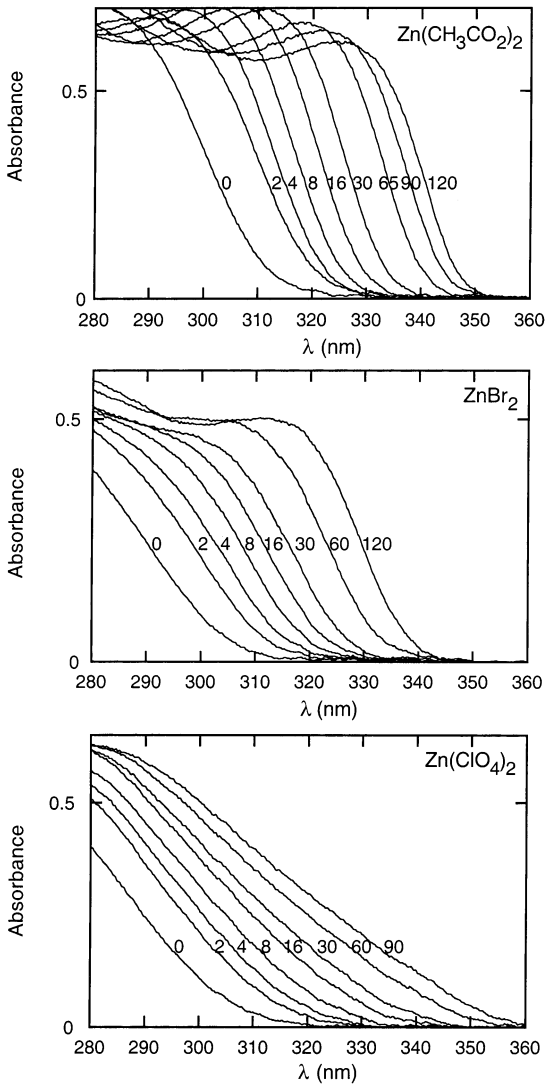

Figure 1. Absorbance spectra for synthesis of ZnO particles from $Zn(CH_3CO_2)_2$, $ZnBr_2$, and $Zn(ClO_4)_2$ in 2-propanol at 35 °C. The time in minutes after mixing the zinc salt solution and the NaOH solution is indicated in each figure.

Results and Discussion

Absorption Spectra. Figure 1 shows absorption spectra for the synthesis of ZnO in 2-propanol at 35 °C from different zinc salts. The spectra for synthesis from $Zn(CH_3CO_2)_2$ solution show a well-defined absorption onset and exciton peak characteristic of solid ZnO immediately after mixing the zinc salt solution and the sodium hydroxide solution, indicating that nucleation is fast. The absorption onset at short times is significantly blue-

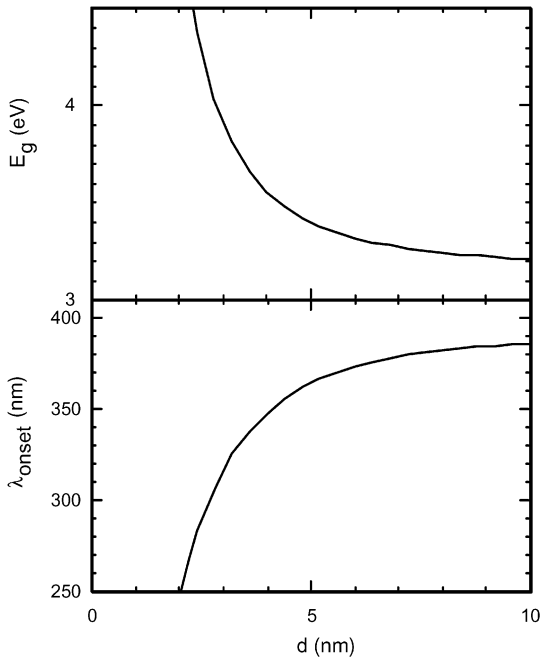

Figure 2. Band gap and absorbance onset versus particle diameter for ZnO.

shifted from the bulk value (about 385 nm) illustrating that the particles are in the quantum regime. The absorption onset red-shifts with time due to increasing particle size. The spectra for synthesis from $ZnBr_2$ solution also show a sharp absorption onset that red-shifts with time, although the exciton peak is not as distinct. Spectra for particle synthesis from $Zn(ClO_4)_2$ show a sharp absorption onset at short times but at longer times the onset becomes broader.

The average particle size in suspension can be obtained from the absorption onset using the effective mass model [e.g., ref 26] where the band gap E_g (in eV) can be approximated by

$$E_g = E_g^{bulk} + \frac{\hbar^2\pi^2}{2er^2}\left(\frac{1}{m_e^* m_0} + \frac{1}{m_h^* m_0}\right) - \frac{1.8e}{4\pi\epsilon\epsilon_0 r} - \frac{0.124e^3}{\hbar^2(4\pi\epsilon\epsilon_0)^2}\left(\frac{1}{m_e^* m_0} + \frac{1}{m_h^* m_0}\right)^{-1} \quad (4)$$

where E_g^{bulk} is the bulk band gap (eV), $\hbar$ is Plank's constant, r is the particle radius, m_e is the electron effective mass, m_h is the hole effective mass, m_0 is free electron mass, e is the charge on the electron, ϵ is the relative permittivity, and ϵ_0 is the permittivity of free space. Due to the relatively small effective masses for ZnO ($m_e = 0.24-0.28$, $m_h = 0.59$ [27,28]), quantum effects are expected to occur for relatively large particle sizes. Figure 2 shows the dependence of the band gap on particle radius according to eq 4 with $E_g^{bulk} = 3.2$ eV, $\epsilon = 8.5$, $m_e = 0.26$, and $m_h = 0.59$. From this figure it is seen that ZnO particles exhibit significant confinement effects for particle diameters less than about 8 nm.

Figure 3 shows the time dependence of the average particle radius obtained from the absorption onset and eq 4 at different temperatures. While there are a number of assumptions in using this method for determining particle size, the validity of this approach was confirmed from analysis of high-resolution transmission electron microscopy (HRTEM) images. For all three zinc salts the initial radius is about 1.5 nm corresponding to a particle with about 190 atoms or about 7 atoms across.

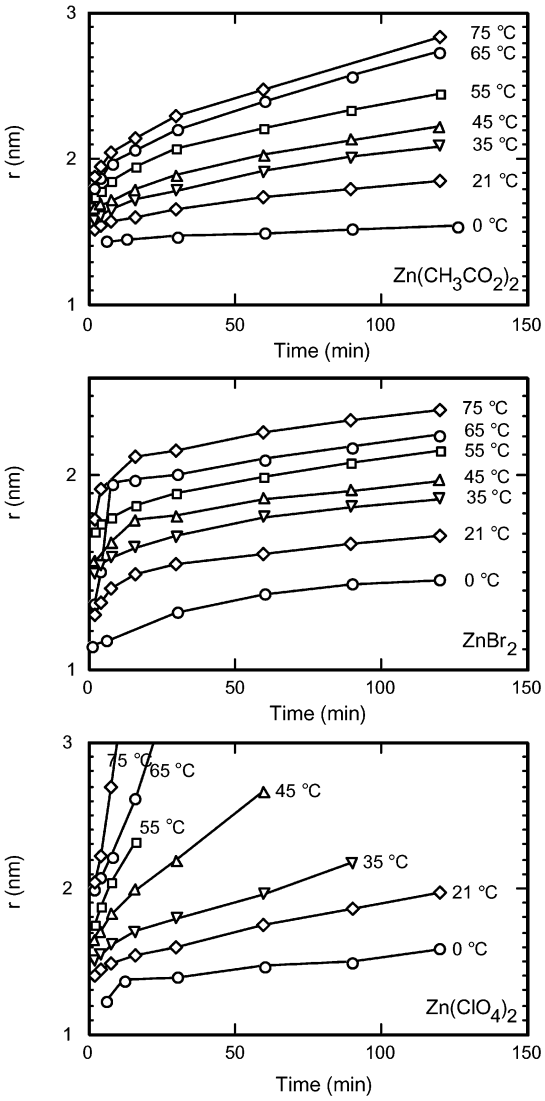

Figure 3. Particle radius versus time for synthesis of ZnO from $Zn(CH_3CO_2)_2$, $ZnBr_2$, and $Zn(ClO_4)_2$ in 2-propanol at 35 °C.

The particle radius versus temperature curves show that particle growth is dependent on both anion and temperature.

Characterization. Figure 4a shows diffraction patterns obtained from the dry powder after rotary evaporation. The ZnO was synthesized from $Zn(CH_3CO_2)_2$ in 2-propanol at 65 °C for 2 h. The powder exhibits the characteristic peaks for the zincite crystal structure along with peaks for orthorhombic sodium acetate.[29] The sodium acetate salt is precipitated during rotary evaporation of the suspension. Sodium acetate is only slightly soluble in alcohol but is very soluble in water (~1.19 g/mL).[30] Figure 4b shows diffraction patterns for the dry powder after repeated washing in water using centrifugation. The diffraction pattern exhibits the characteristic zincite peaks and shows no evidence of crystalline sodium acetate, indicating that it was completely removed using the washing procedure.

Figure 5 shows HRTEM images of ZnO particles synthesized from $Zn(CH_3CO_2)_2$ at 55 °C after 8.5 h. The images show that the particles are approximately spherical and from the lattice fringes it can be seen that the particles are single crystal and that many exhibit some faceting. From analysis of many images we determine an average diameter of 6.5 ± 1.2 nm (289 particles). From the absorption spectrum, shown in Figure 6, we obtain an average particle diameter of 6.9 nm, although from Figure 2 it is seen that this is in the range of particle sizes where

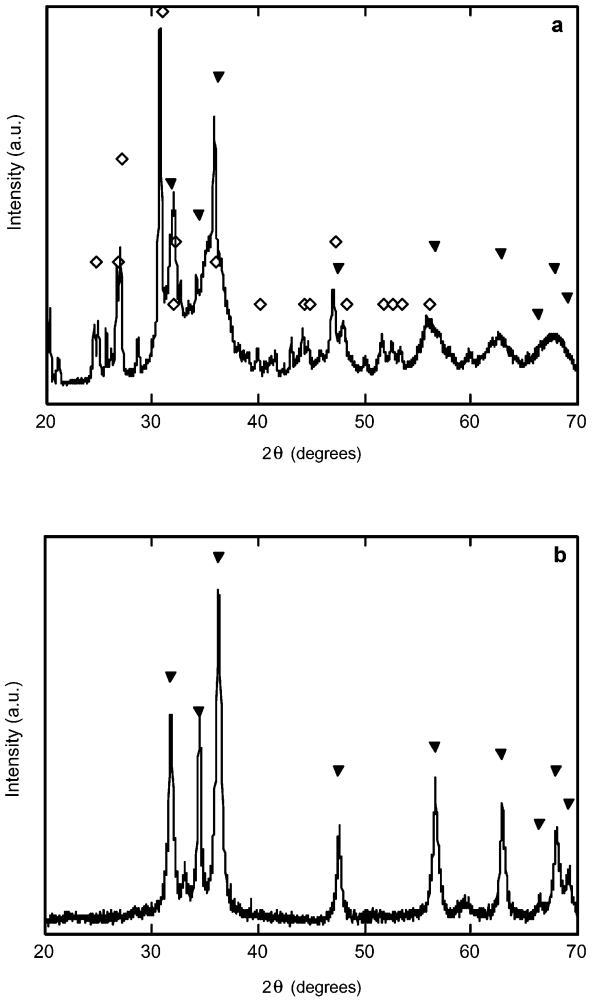

Figure 4. X-ray diffraction patterns for ZnO synthesized from $Zn(CH_3CO_2)$ in 2-propanol at 65 °C for 2 h. (a) ZnO powder after rotary evaporation, and (b) ZnO powder after sequential washing in water. (▽) zincite and (◇) sodium acetate peaks (from ref 29); height indicates relative intensity.

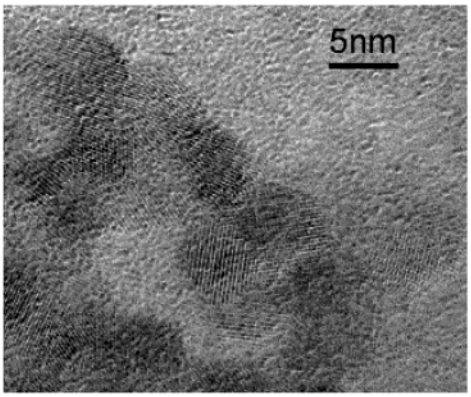

Figure 5. HRTEM image of ZnO particles synthesized from $Zn(CH_3CO_2)_2$ at 55 °C for 8.5 h.

the band gap enlargement is small and hence the error in determining the particle size is relatively large.

Figure 7 shows HRTEM images of two ZnO particles synthesized in $ZnBr_2$ solution at 55 °C for 8.5 h. The particles are approximately spherical but show evidence of faceting. From several images we determine an average particle diameter of 4.9 ± 0.8 nm (63 particles). From the absorption spectrum, shown in Figure 6, we obtain an average particle diameter of 5.0 nm, in good agreement with the value obtained from

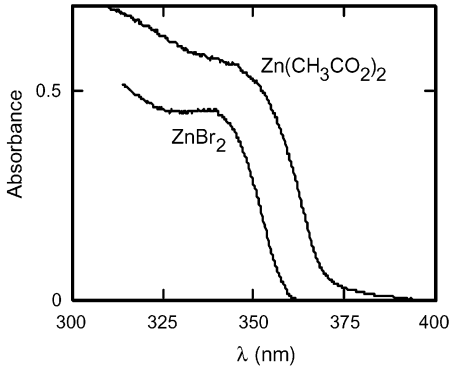

Figure 6. Absorbance spectra for synthesis of ZnO particles from $Zn(CH_3CO_2)$ and $ZnBr_2$ in 2-propanol at 55 °C after 8.5 h. Spectra correspond to suspensions from which HRTEM images were obtained.

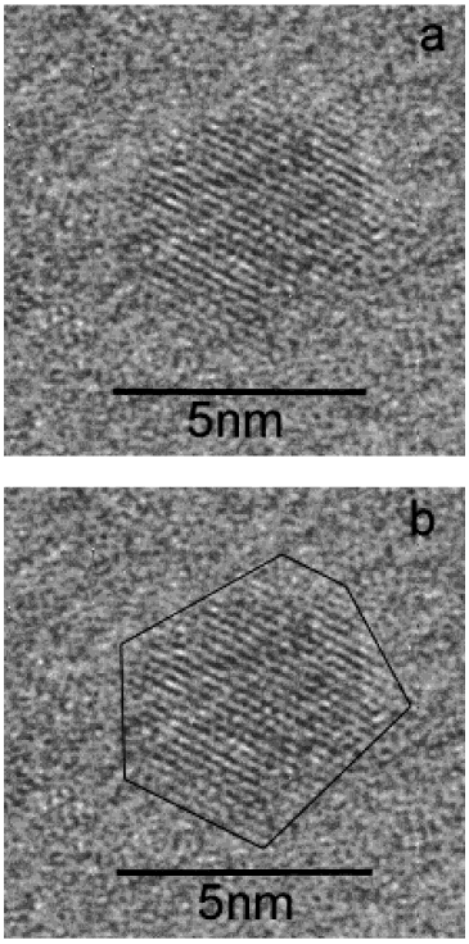

Figure 7. (a) HRTEM image of ZnO particle synthesized from $ZnBr_2$ at 55 °C for 8.5 h. (b) Image from (a) showing the perimeter of the particle.

HRTEM images. Figure 6 shows that there is a significant difference in the absorption onset for particles synthesized from $ZnBr_2$ compared to particles synthesized from $Zn(CH_3CO_2)_2$ for the same time and at the same temperature.

Figure 8 shows an image of a ZnO particle grown from $Zn(ClO_4)_2$ at 55 °C after 40 min. The images show elongated and irregularly shaped particles. From the lattice fringes it is clear that these particles are single crystals implying that they are formed by epitaxial attachment of several smaller particles. Note that this time and temperature correspond to the regime where the suspensions become translucent (see Figure 3).

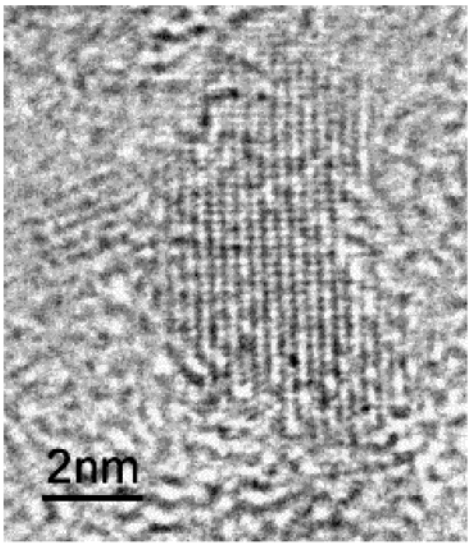

Figure 8. HRTEM image of a ZnO particle synthesized from $Zn(ClO_4)_2$ at 55 °C for 40 min.

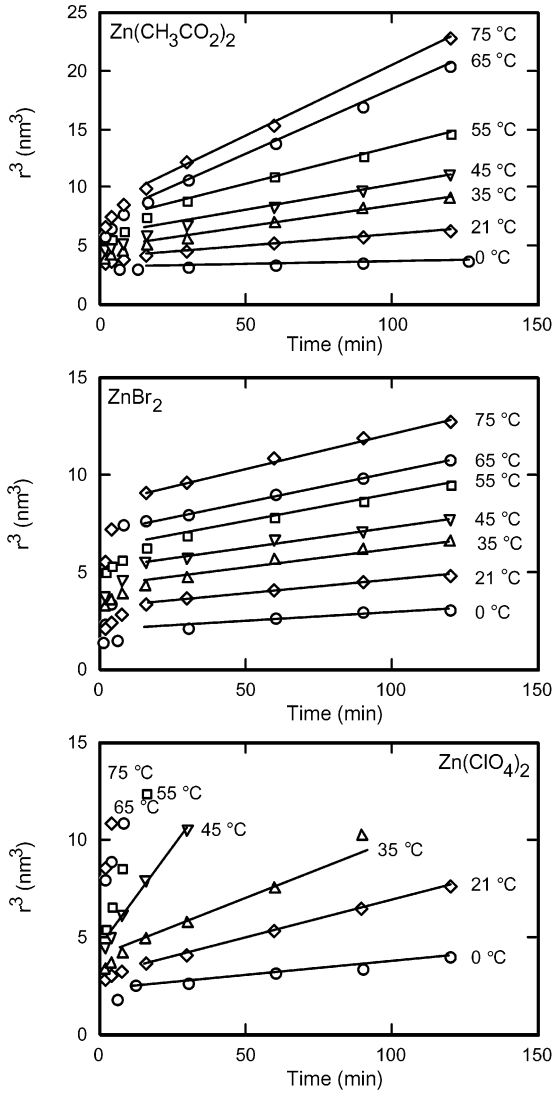

Figure 9. Particle radius versus time curves from Figure 3 plotted as r^3 versus time.

Growth Kinetics. Figure 9 shows the average particle radius from Figure 3 replotted as $\bar{r}^3$ versus time. Figures 9a and 9b show that soon after nucleation the increase in average particle size in $Zn(CH_3CO_2)_2$ and $ZnBr_2$ follows the rate law for diffusion-limited coarsening over the measured temperature range from 0 °C to 75 °C. ZnO synthesis from $Zn(ClO_4)_2$ (Figure 9c) follows eq 2 at low temperatures and short times but at longer times the particle size increases sharply.

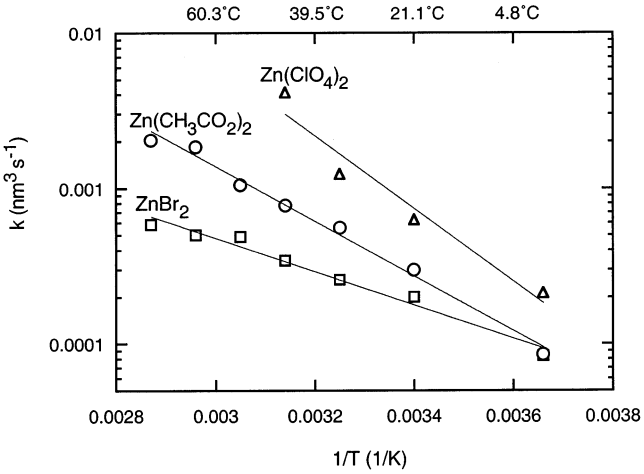

Figure 10. Arrhenius plot of the rate constant for the coarsening of ZnO particles from $Zn(CH_3CO_2)_2$, $ZnBr_2$, and $Zn(ClO_4)_2$ in 2-propanol.

These results indicate that particle growth is completed shortly after nucleation so that at longer times the increase in particle size is determined solely by diffusion-limited coarsening for synthesis from $Zn(CH_3CO_2)_2$ and $ZnBr_2$. For the case of $Zn(ClO_4)_2$ the regime where coarsening is observed is limited to particle radii up to about 2 nm. At longer times the particle radius increases more rapidly than for coarsening, due to epitaxial cluster aggregation, as shown in the HRTEM image in Figure 8. Epitaxial attachment results in the generation of particles much larger than the average particle size since the particle size can effectively double when two particles of similar size attach. These larger particles significantly broaden the size distribution resulting in both a red shift and broadening of the absorption onset. We note that random aggregation is not expected to lead to a red-shift in the absorbance spectra due to the weak electronic coupling between particles. Figure 9 shows that the onset of the rapid increase in particle size is dependent on temperature and occurs at a particle radius of about 2 nm in all cases suggesting that particles must exhibit sufficient faceting for epitaxial attachment to occur. We also note that the $Zn(ClO_4)_2$ suspensions became translucent at longer times, after the rapid increase in particle size.

From Figure 9 it is seen that the coarsening rate is dependent on the anion. At any temperature the coarsening rate of ZnO particles is fastest for synthesis from $Zn(ClO_4)_2$ and is slowest from $ZnBr_2$. The decrease in coarsening rate from $Zn(ClO_4)_2$ to $Zn(CH_3CO_2)_2$ to $ZnBr_2$ is consistent with the tendency for the anion to adsorb on a surface. In general, halide ions adsorb more strongly on surfaces than acetate ions, and perchlorate ions exhibit very weak surface interactions.[31] In the gas phase, acetic acid is known to displace ethanol and dissociatively adsorb on ZnO surfaces,[32] and hence it is not surprising that acetate ions are adsorbed on the surface of the particles in propanol.

The rate constant for coarsening k can be obtained from the slopes of the linear regions of the plots of r^3 versus time. Figure 10 shows the rate constant obtained from the three salts on an Arrhenius plot. It is seen that the rate constant is in the range $10^{-4}-10^{-2}$ nm^3 s^{-1} and increases with increasing temperature. At higher temperatures it is evident that the rate constant is largest for coarsening from $Zn(ClO_4)_2$ and smallest for coarsen-

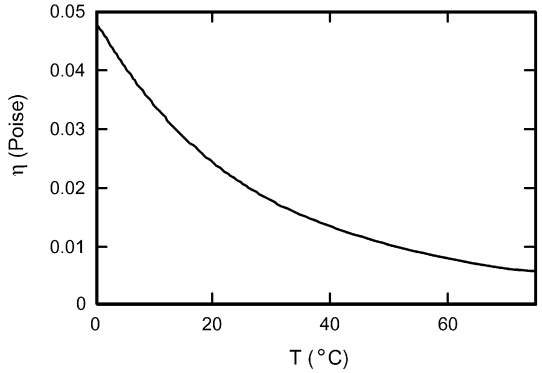

Figure 11. Viscosity of 2-propanol versus temperature.

ing from $ZnBr_2$. The activation energies obtained from the slopes are 0.21 eV for coarsening from $ZnBr_2$, 0.35 eV for coarsening from $Zn(CH_3CO_2)_2$, and 0.46 eV for coarsening from $Zn(ClO_4)_2$ solution.

The rate constant k is given by

$$k = \frac{8\gamma D V_m^2 c_{r=\infty}}{9RT} \quad (5)$$

where γ is the surface energy, D is the diffusion coefficient, V_m is the molar volume, and $c_{r=\infty}$ is the equilibrium concentration at a flat surface (i.e. the bulk solubility). The temperature dependence of the rate constant can be considered by eliminating the diffusion coefficient from eq 5. From the Stokes−Einstein equation:

$$D = \frac{k_B T}{6\pi\eta a} \quad (6)$$

where k_B is the Boltzmann constant, η is the viscosity of the solvent, and a is the solvated ion radius. Substituting into eq 6 we obtain

$$k = \frac{8\gamma V_m^2 c_{r=\infty}}{54\pi\eta a N_A} \quad (7)$$

Thus the rate constant for particle coarsening is a function of γ (the surface energy of the crystal), V_m (the molar volume), $c_{r=\infty}$ (the bulk solubility), η (the solvent viscosity), and a (the solvated ion radius). V_m for ZnO is 14.8 $cm^3\ mol^{-1}$ and is essentially constant over the temperature range of interest since the linear expansion coefficient is about $4 \times 10^{-6}\ K^{-1}$ over a wide temperature range.[30] The surface energy for the solid−vapor interface for metal oxides is on the order of 1 $J\ m^{-2}$,[33−35] however, adsorption of ions and solvent molecules is expected to reduce the surface energy of the solid−liquid interface to values in the range 0.1−0.5 $J\ m^{-2}$.[36] The solvated ion radius for Zn^{2+} in ethanol is 0.51 nm and is independent of temperature.[37] The viscosity of 2-propanol exhibits a relatively strong dependence on temperature, decreasing from about 5 cp at 0 °C to about 0.5 cp at 75 °C,[38] as shown in Figure 11.

The influence of viscosity on the temperature dependence of the rate constant can be seen from Figure 12 which shows a plot of the product $k\eta$ versus $1/T$. Figure 12 shows that $k\eta$ for coarsening from $ZnBr_2$ is almost independent of temperature while coarsening from $Zn(CH_3CO_2)_2$ exhibits a very weak temperature dependence. From these results we conclude that the temperature dependence of the rate constant is dominated by the temperature dependence of the viscosity which, in turn, controls the ion diffusion rate. The temperature dependence of

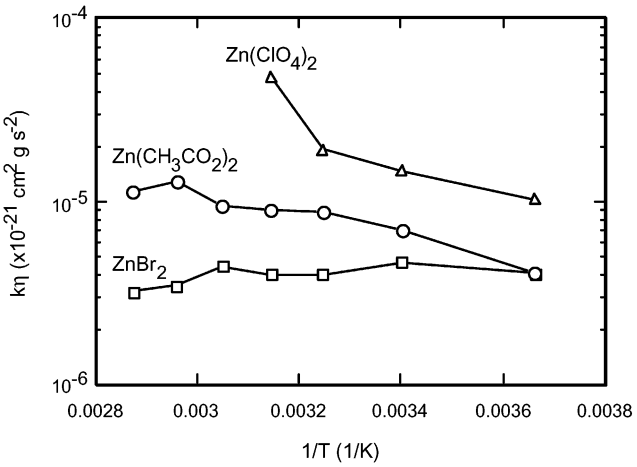

Figure 12. Arrhrenius plot of $k\eta$ for the synthesis of ZnO particles from $Zn(CH_3CO_2)_2$, $ZnBr_2$, and $Zn(ClO_4)_2$ in 2-propanol.

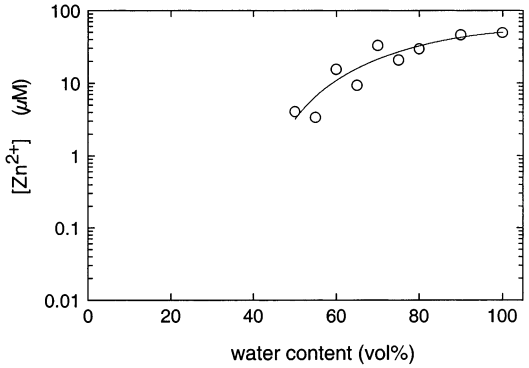

Figure 13. Solubility of ZnO in 2-propanol/water solutions.

$k\eta$ shown in Figure 12 is due to the temperature dependence of the bulk solubility $c_{r=\infty}$ and from the slopes it can be inferred that the activation energy for dissolution of ZnO is smallest in ClO_4^- and largest in Br^-.

Since γ, V_m, a, and η are known, the bulk solubility $c_{r=\infty}$ can be estimated from the experimentally determined rate constants using eq 5. The rate constant varies from 10^{-4} to 10^{-3} $nm^3\ s^{-1}$. Taking the viscosity from Figure 10 and using γ = 0.1 $J\ m^{-2}$, a = 0.51 nm, and V_m = 14.8 $cm^3\ mol^{-1}$, the bulk solubility is determined to be in the range 10^{-11}−10^{-9} M. Verification of the bulk solubility is very difficult due to the very low concentrations. However, the solubility in water is relatively large so that an estimate can be obtained from extrapolation of the solubility in 2-propanol/water solutions.

Figure 13 shows the solubility of ZnO in 2-propanol/water solutions obtained from atomic absorption spectroscopy. Special care was taken to make sure that only dissolved Zn(II) was present in the sample (see Experimental section). In water, the Zn(II) concentration is 49×10^{-6} M, in good agreement with values reported in the literature.[39] On increasing the concentration of propanol in the water/propanol mixture, the Zn(II) concentration decreased, and at about 60% water the concentration was below the detection limit of 1×10^{-6} M. To our knowledge, there is no quantitative description for the solubility of metal oxides in alcohol/water mixtures. Extrapolation of the solubility to zero water content gives values in the range 10^{-11} to 10^{-7} M, consistent with the values of 10^{-11} to 10^{-9} M obtained from the rate constant. These results suggest that the solubilities obtained from the rate constant are of similar magnitude to the values obtained from extrapolation of the solubility curve in Figure 12.

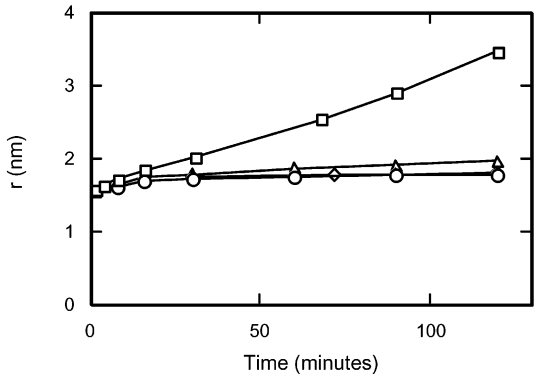

Figure 14. Particle radius versus time for synthesis of ZnO particles in 2-propanol at 45 °C from (□) $Zn(ClO_4)_2$ + NaOH, (○) $ZnBr_2$ + NaOH, (◇) $Zn(ClO_4)_2$ + NaOH + NaBr, and (Δ) $ZnBr_2$ + NaOH + $NaClO_4$.

As described above, the decrease in rate constant for coarsening from $Zn(ClO_4)_2$ to $Zn(CH_3CO_2)_2$ to $ZnBr_2$ is consistent with the tendency for the anion to adsorb on a surface. This is supported by the results shown in Figure 14 illustrating that the addition of $NaBr_2$ to $Zn(ClO_4)_2$ results in growth kinetics characteristic of $ZnBr_2$. Similarly, the addition of $NaClO_4$ to $ZnBr_2$ also results in growth kinetics characteristic of $ZnBr_2$. Furthermore, epitaxial attachment is only expected to be important for systems with no adsorbed layer. Thus, the observation of epitaxial attachment from $Zn(ClO_4)_2$ solution is consistent with the fact that ClO_4^- is not expected to adsorb on the ZnO surface.

Conclusions

The synthesis of ZnO nanoparticles from $Zn(CH_3CO_2)_2$, $ZnBr_2$, and $Zn(ClO_4)_2$ in 2-propanol is characterized by fast nucleation and growth followed by diffusion-limited coarsening. For the case of $Zn(ClO_4)_2$, coarsening is observed at shorter times whereas at longer times epitaxial attachment leads to a rapid increase in particle diameter. The rate constant for coarsening at constant temperature increases in the order $Br^- < CH_3CO_2^- < ClO_4^-$, indicating that the rate is dependent on anion adsorption. The temperature dependence of the rate constant for coarsening is due to the temperature dependence of the solvent viscosity and the temperature dependence of the bulk solubility of ZnO.

Acknowledgment. The authors gratefully acknowledge support from the JHU MRSEC (NSF Grant DMR00-80031).

References and Notes

(1) Henglein, A. *Top. Curr. Chem.* **1988**, *143*, 113.
(2) Livage, J.; Henry, M.; Sanchez, C. *Prog. Solid State Chem.* **1988**, *18*, 259.
(3) Matijevic, E. *Langmuir* **1986**, *2*, 12.
(4) Sugimoto, T. *Adv. Colloid Interface Sci.* **1987**, *28*, 65.
(5) Murray, C. B.; Kagan, C. R.; Bawendi M. G. *Annu. Rev. Mater. Sci.* **2000**, *30*, 545.
(6) Steigerwald, M. L.; Brus, L. E. *Acc. Chem. Res.* **1990**, *23*, 183.
(7) Murray, C. B.; Norris, D. J.; Bawendi, M. G. *J. Am. Chem. Soc.* **1993**, *115*, 8706.
(8) Bowen Katari, J. E.; Colvin, V. L.; Alivisatos, A. P. *J. Phys. Chem.* **1994**, *98*, 4109.
(9) Rosetti, R.; Hull, R.; Gibson, J. M.; Brus, L. E. *J. Chem. Phys.* **1985**, *83*, 1406.
(10) Peng, X.; Wickham, J.; Alivisatos, A. P. *J. Am. Chem. Soc.* **1998**, *120*, 5343.
(11) Olshavsky, M. A.; Goldstein, A. N.; Alivisatos, A. P. *J. Am. Chem. Soc.* **1990**, *112*, 9438.
(12) Kormann, C.; Bahnemann, D. W.; Hoffmann, M. R. *J. Phys. Chem.* **1988**, *92*, 5196.
(13) Bahnemann, D. W.; Kormann, C.; Hoffmann, M. R. *J. Phys. Chem.* **1987**, *91*, 3789.
(14) Sphanel, L.; Anderson, M. A. *J. Am. Chem. Soc.* **1991**, *113*, 2826.
(15) Kamat, P. V.; Patrick, B. *J. Phys. Chem.* **1992**, *96*, 6829.
(16) Leland, J. K.; Bard, A. J. *J. Phys. Chem.* **1987**, *91*, 5076.
(17) Hardee, K. L.; Bard, A. J. *J. Electrochem. Soc.* **1977**, *124*, 215.
(18) Lifshitz, I. M.; Slyozov, V. V. *J. Phys. Chem. Solids* **1961**, *19*, 35.
(19) Wagner, C. *Z. Elektrochem.* **1961**, *65*, 581.
(20) Penn, R. L.; Banfield, J. F. *Science* **1998**, *281*, 969.
(21) Banfield, J. F.; Welch, S. A.; Zhang, H.; Thomsen Ebert, T.; Penn, R. L. *Science* **2000**, *289*, 751.
(22) Alivisatos, A. P. *Science* **2000**, *289*, 736.
(23) Penn, R. L.; Oskam, G.; Strathmann, J.; Searson, P. C.; Stone, A. T.; Veblen, D. R. *J. Phys. Chem.* B **2001**, *105*, 2177.
(24) Wong, E. M.; Bonevich, J. E.; Searson, P. C. *J. Phys. Chem. B* **1998**, *102*, 7770.
(25) Bahnemann, D. W.; Kormann, C.; Hoffmann, M. R. *J. Phys. Chem.* **1987**, *91*, 3789.
(26) Brus, L. E. *J. Phys. Chem.* **1986**, *90*, 2555.
(27) Shionoya, S. In *Phosphor Handbook*; Shionoya, S., Yen, W. M., Eds.; CRC Press: Boca Raton, 1998.
(28) Berger, L. I. *Semiconductor Materials*; CRC Press: Boca Raton, 1997; p 184.
(29) Adamson, A. W. *Physical Chemistry of Surfaces*, 5th ed.; Wiley: New York, 1990.
(30) Spitz, R. N.; Barton, J. E.; Barteau, M. A.; Staley, R. H.; Sleight, A. W. *J. Phys. Chem.* **1986**, *90*, 4067.
(31) JCPDS diffraction database, orthorhombic β-$NaC_2H_3O_2$ (29-1158), zincite (36-1451).
(32) *CRC Handbook of Chemistry and Physics*, 72nd ed.; CRC Press: Boca Raton, 1991.
(33) Wang, X. G.; Weiss, W.; Shaikhutdinov, Sh. K.; Riter, M.; Petersen, M.; Wagner, F.; Schlogl, R.; Scheffler, M. *Phys. Rev. Lett.* **1998**, *81*, 1038.
(34) Manassidis, I.; De Vita, A.; Gillan, M. J. *Surf. Sci. Lett.* **1993**, *285*, L517.
(35) Weirauch, D. A.; Ownby, P. D. *J. Adhesion. Sci. Technol.* **1999**, *13*, 1321.
(36) Zangwill, A. *Physics at Surfaces*; Cambridge University Press: Cambridge, 1988.
(37) Lovas, R.; Macri, G.; Petrucci, S. *J. Am. Chem. Soc.* **1970**, *92*, 6502.
(38) *Electrolyte Data Collection, Part 3: Viscosity of Nonaqueous Solutions I: Alcohol Solutions*; Barthel, J., Neueder, R., Meier, R., Eds.; Chemistry Data Series, Vol. XII, Part 3, Dechema: Frankfurt, Germany, 1997.
(39) Remy, H. *Z. Elektrochem. Angew. Physik. Chem.* **1925**, *31*, 88.